Cytometry
PART A
Journal of the International Society for Advancement of Cytometry

# Observation of Calcium Microdomains at the Uropod of Living Morphologically Polarized Human Neutrophils Using Flash Lamp-Based Fluorescence Microscopy

**Andrea J. Clark,[1] Howard R. Petty[1,2]***

[1]Department of Ophthalmology and Visual Sciences, The University of Michigan Medical School, Ann Arbor, Michigan 48105

[2]Department of Microbiology and Immunology, The University of Michigan Medical School, Ann Arbor, Michigan 48105

Received 24 December 2007; Revision Received 19 March 2008; Accepted 15 April 2008

Contract grant sponsors: NCI and the Wilson Medical Foundation.

*Correspondence to: Dr. Howard R. Petty, Department of Ophthalmology and Visual Sciences, 1000 Wall Street, The University of Michigan Medical School, Ann Arbor, MI 48105, USA

Email: hpetty@umich.edu

Published online 21 May 2008 in Wiley InterScience (www.interscience.wiley.com)

DOI: 10.1002/cyto.a.20580



## Abstract

The present study outlines improved strategies for ratiometric imaging of cell calcium using a flash lamp-based excitation method and its application to neutrophil polarization. A brief (~6 $\mu$s) and intense flash was used to excite the Fluo-4 and Fura Red calcium dye combination in morphologically polarized human neutrophils. These illumination conditions do not allow the dye or calcium ions to diffuse significant distances during the exposure period. Buffer conditions such as pH, pyruvate concentration, and glucose levels were adjusted to more faithfully replicate these parameters in sepsis patients. Fluorescence images at both dyes' emission wavelengths were simultaneously collected using a Dual-View apparatus and an ICCD camera. The ratiometric images, when viewed as single frames or averaged image stacks, clearly demonstrated high calcium probe ratios at the uropod and comparatively low ratios at the cell body that were not evident using conventional imaging methods with longer exposure times. Calcium signaling at the uropod is likely associated with cytoskeletal remodeling during cell motility. © 2008 International Society for Advancement of Cytometry

## Key terms

neutrophil; motility; imaging; calcium microdomains; uropod

**THERE** is general agreement that $Ca^{2+}$ ions play key roles in chemical signaling within cells (e.g., 1–6). Cytosolic $Ca^{2+}$ signals arise from $Ca^{2+}$ entering a cell from the extracellular milieu and from the intracellular release of stored $Ca^{2+}$. These two broad classes of $Ca^{2+}$ entry pathways are supported by several distinct molecular machineries. For example, extracellular $Ca^{2+}$ entry can be mediated by voltage-gated and nonvoltage-gated membrane channels. The release of $Ca^{2+}$ from internal stores is carried out by multiple organelles utilizing multiple signaling and channel mechanisms. Examples of these systems include inositol trisphosphate, sphingosine-1-phosphate, and cyclic ADP-ribose. Not only is there substantial heterogeneity in the receptors, signaling mechanisms, and intracellular second messengers mediating $Ca^{2+}$ signals, but there also appears to be a great variety of $Ca^{2+}$ signals, as judged by the heterogeneity of physiological outcomes.

These heterogeneous $Ca^{2+}$ signals are conventionally imaged with fluorescence microscopes using cameras with total acquisition times for one ratio image on the order of seconds. As solvated ions and small molecules have diffusion coefficients of $\sim 10^{-5}$ cm$^2$/sec, spatial and temporal information contained within the image are blurred during the exposure period. Indeed, diffusion coefficients spanning the range reported for $Ca^{2+}$ ($1.3 \times 10^{-7}$ to $10^{-5}$ cm$^2$/s) (e.g., 7–9) yield root-mean-squared (rms) displacements during a one second exposure time that are roughly equal to the size of a cell or greater (5–45 $\mu$m). Consequently, the underlying heterogeneity in $Ca^{2+}$ signaling mechanisms is not registered in the observed images. One strategy to minimize diffusional blurring is to use pulsed lasers or flash lamps to excite a sample

ISAC
International Society for Advancement of Cytometry

during frame acquisition. The principle behind this approach is the same as using strobe lights in high-speed photography. Using this approach, intracellular $Ca^{2+}$ signaling has been observed in stimulated chromaffin cells and skeletal muscle (10–14). In the present study we report improved methodologies to study $Ca^{2+}$ signaling that rely upon a flash lamp-based excitation source. In our studies the exposure time is 6 $\mu$s, which leads to rms displacements that are smaller than the Rayleigh criterion for microscopic resolution for diffusion coefficients of $<10^{-5}$ $cm^2/s$. This approach is used to study $Ca^{2+}$ signaling in polarized neutrophils. In contrast to previous studies of human neutrophils, our data indicate that $Ca^{2+}$ release within polarized cells is primarily associated with the uropod.

## Materials and Methods

### Materials

Fura Red-AM (cat. # 3021), Fluo-4-AM (cat. # F23917), Pluronic-F127 (cat. # P6866), cell media, and phosphate buffered saline (PBS) were obtained from Invitrogen Corp. (Carlsbad, CA). Ficoll-Histopaque and all other chemicals were obtained from Sigma Chemical Company (St. Louis, MO). Excitation and emission filter sets were obtained from Chroma Technology Corp. (Rockingham, VT).

### Cell Preparation

Peripheral blood was collected from healthy human donors in compliance with the guidelines of the University of Michigan Institutional Review Board for Human Subject Research. Neutrophils were isolated using Ficoll-Histopaque density gradient centrifugation then re-suspended and washed in PBS by centrifugation. Cell viability was checked with Trypan Blue exclusion and by morphological examination.

### Cell Labeling for $Ca^{2+}$ Imaging and Recording

Cells were labeled with a dye pulse-chase protocol to provide optimal labeling and minimal dye leakage during experiments. Cells were incubated with 5.5 $\mu$M Fura Red, 2.6 $\mu$M Fluo-4 and 2 % Pluronic-F127 in PBS for 1 h at 37°C. After incubation, cells were washed with PBS, resuspended in $Ca^{2+}$ imaging buffer and incubated for a further 30 min at 37°C, to purge excess dye. Cells were washed with imaging buffer before use.

### Imaging Buffer

The imaging buffer was composed of the following components: 150 mM NaCl, 4 mM KCl, 25 mM HEPES, 3 mM $CaCl_2$, 5 mM pyruvate, 10 mM glucose, and 1 mg/ml bovine serum albumin (BSA). The pH was adjusted to 7.9. Osmolarity was adjusted to ~300 mOsm using a $\mu$Osmette osmometer (Precision Systems, Natick, MA).

This imaging buffer was designed to better replicate the physiological conditions associated with inflammatory disease. This slightly higher pH corresponds more closely to the pH of arterial blood early in the sepsis response (pH7.6) (15) as well as to certain tissues (16). A glucose concentration of 10 mM was also chosen to match that observed in septic patients (17). In addition, pyruvate is a known regulator of $Ca^{2+}$ signaling (18) that is elevated in sepsis (17). As the concentration of this small organic anion is expected to rapidly decline *in vitro* (e.g., 18), we have included pyruvate in the imaging buffer to more closely simulate metabolic conditions within tissues.

### Conventional Imaging

Conventional fluorescence microscopy was performed using a Nikon TE2000 Quantum inverted microscope (Nikon Instruments, Inc., Melville, NY). A continuous mercury lamp attached to the microscope via a dual port adaptor was employed (Nikon). Two filter cubes (Chroma Technology Corp.) were used to collect images. For Fluo-4, a cube containing an HQ475/40x excitation filter, a 510 nm dichroic beamsplitter, and an HQ530/30m emission filter were used. For Fura Red, an HQ475/40x excitation filter, a 510 nm dichroic beamsplitter, and an HQ670/50m emission filter were used. Images with these filter sets were sequentially collected via the bottom microscope port using a back-illuminated iXon (DV887) cooled electron multiplying charge-coupled device camera (EMCCD) (Andor Technology, South Windsor, CT). A threshold was applied (19) then ratio images were calculated using MetaFluor (Molecular Devices, Danville, PA) software.

### Instrumentation for Flash Lamp-Based System

The overall instrument set-up is shown in Figure 1. Excitation was provided by a FX-4400 xenon flash lamp, LitePac and PS-4400 power supply (Perkin-Elmer Optoelectronics, Salem, MA); the lamp has an output from 275 to 2,000 nm. The output of the PS-4400 was set to 950 V. The electromagnetic interference of the lamp and associated electronics were judged to be insignificant in the laboratory environment. An aluminum housing was constructed to hold the flash lamp and bulb to the filter unit and microscope. To reduce the UV and IR components of the emission, an Oriel water filter and a KG-1 Schott filter were used. The water filter, which was filled and cleaned regularly, utilized quartz windows; it provides a roughly $10^9$-fold attenuation of the UV and IR relative to the visible light. As the lamp was bright, attenuation of the visible was not an issue with the Schott filter. The excitation source was coupled to a Nikon TE-2000 inverted microscope. To simultaneously excite Fluo-4 to Fura Red, an HQ475/40x excitation filter and a 510-nm dichroic beamsplitter were used. To simultaneously collect emission images at two emission wavelengths, a Dual-View apparatus (Optical Insights, Tuscon, AZ) was employed. In these experiments emission bands were selected with a 600-nm dichroic reflector in conjunction with an HQ530/30 m filter for Fluo-4 emission and an HQ670/50m filter for Fura Red emission. A Princeton Instruments PI-Max II intensified CCD detector (Gen3 with 1Kx1K chip) was used at a gain setting of 255. The camera was attached to the Dual-View emission image-splitting device. The camera and flash lamp were synchronized: the flash was triggered while the camera

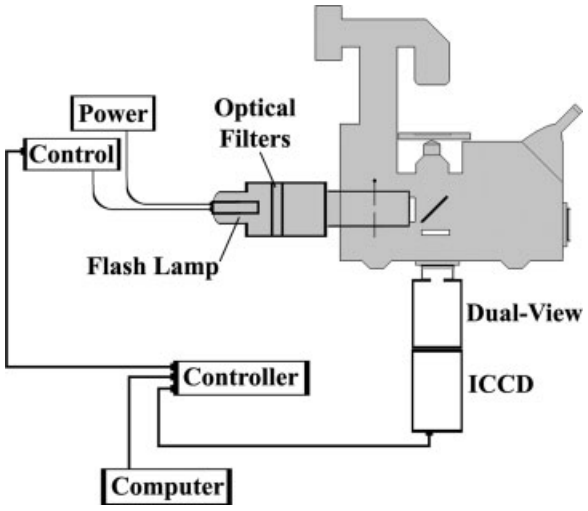


**Figure 1.** Flash lamp-based ratiometric microscope imaging system. A schematic representation of the microscope system is shown. The FX-4400 flash lamp and socket utilize a PS-4400 power supply (shown) and a 24V DC source (not shown). The flash lamp generates a brief, intense pulse of light. This is attached to the microscope via a coupling device that includes a water filter and slots for insertion of other filters, such as a KG-1 Schott filter and excitation filters. The fluorescence emission is collected at a 100% side port (shown here as a bottom port to simplify the illustration). The emission light is split by the Dual-View apparatus then imaged by an ICCD camera.

was on yielding an image stack where each frame is a dual image associated with a single flash of the lamp.

### Data Collection and Processing

Neutrophils were placed on a 37°C heated stage in a cover-glass bottom dish. A Nikon 100x/1.45na plan apochromat objective was used to maximize light collection. Cells were imaged at 8 frames per second, which allowed a complete one megapixel file to be downloaded. Frame rates can be increased using horizontal ROIs. WinSpec files containing Dual-View images at both wavelengths were imported using a cross-over cable onto another computer running MetaMorph (Molecular Devices) where the images were split and reformatted. The new file format enables the files to be opened in MetaFluor (Molecular Devices), where a ratio (Fluo-4/Fura Red) image is produced and analyzed. A threshold was applied to images of each dye in order to restrict ratio calculation to within the cell boundaries. To visualize the results, color LUTs were employed.

## Results

In the present study we test the hypothesis that enhanced $Ca^{2+}$ signaling can be observed at the uropod of polarized neutrophils using improved experimental protocols. To accomplish this goal, we have developed a system using a flash lamp source for very brief exposure times in conjunction with simultaneous emission detection at two wavelengths (Fig. 1) while minimizing noise sources (e.g., 20). To further enhance the signal-to-noise ratio, we have employed the probes Fluo-4 and Fura Red in conjunction with a 30-min wash period; this minimizes the leakage of unmodified and partially modified probes from cells during experiments. In addition to these physical and chemical strategies, we have also employed an improved imaging buffer for these experiments (see Materials and Methods).

To test our hypothesis as well as the modified experimental tools, we have studied polarized neutrophils labeled with Fluo-4 and Fura Red. Cells were pulse-chase labeled with these probes as described above, washed with imaging buffer, and then placed on glass coverslips for microscopic examination. In the first experiment, conventional imaging approaches were used. Figure 2A–2F shows DIC images, fluorescence images, and line profile analyses of a polarized neutrophil collected at two different time points. In this case, Fluo-4 and Fura Red images were sequentially collected for 500 ms each using an EMCCD camera. The conventional ratio micrographs (Fig. 2B and 2E) show that the center of the cell body is the highest Fluo-4/Fura Red ratio region of the cell. Some enhancement in the fluorescence ratio is also apparent at the uropod (Fig. 2B). Although the line profile analyses are dominated by the broad, intense cell center, Figure 2C shows that some enhanced intensity is also apparent at the uropod using conventional imaging methodology, suggesting that improvements in cell labeling and buffers also contribute to the improved $Ca^{2+}$ pattern detection. As cell morphology changes and the uropod disappears, the $Ca^{2+}$ signal in this region is reduced (Fig. 2E, 2F). Cells that were not morphologically polarized did not display enhanced $Ca^{2+}$ signaling at the uropod (Fig. 3A).

When probe diffusion was removed using flash lamp-based excitation, different results were obtained: the cell body exhibited a lower Fluo-4/Fura Red ratio in comparison to the uropod. Flash lamp-based excitation was employed to obtain the images shown in Figure 2G–2L. To facilitate comparison of conventional and high speed photomicrographs, all of the images of Figure 2 were collected from the same cell, thus differences cannot be ascribed to cell-to-cell variability. The images of panels G–L were collected between the exposures of panels B and E; we thereby bracketed the flash lamp-based acquisition with conventional illumination experiments. Single frames associated with individual flashes of the FX-4400 lamp are shown in panels G–I. Panel H clearly shows that the uropod displays a much higher Fluo-4/Fura Red ratio than other regions of the cell. Additional frames of images acquired near the frames of panels G, H, and I were compressed into the single images shown in panels J, K, and L. Panel K shows an intense fluorescence ratio signal in the region of the uropod. Some enhanced signal in this region may also be noted in panels J and L. Interestingly, panel K also displayed a higher Fluo-4/Fura Red ratio near the cell periphery at the lamellipodium in comparison to the cell body. To further illustrate these results, line profile analyses were performed. Figure 2M–2O shows line profile analyses of high speed micrographs. Figure 2K shows clearly the uropod exhibits a high fluorescence ratio and therefore suggests that some enhancement of the $Ca^{2+}$ signal at the lamellipodium is also present. Hence, flash lamp-

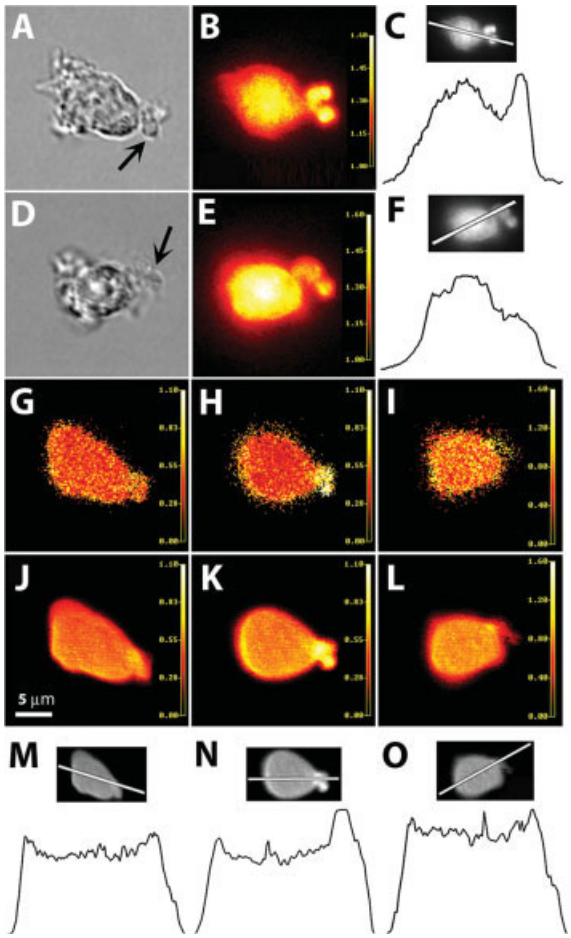


**Figure 2.** Ratio imaging microscopy of a polarized neutrophil collected with multiple imaging modalities. The same cell is shown in all panels of this figure. These data were obtained in the sequence: **A-G(J)-B(C)-H(K)-I(L)-D-E(F)**. Panels A-G(J)-B-H(K) were collected in roughly 5 min; the remainder were collected roughly 25 min later. DIC micrographs are shown in panels A and D for different time points. The corresponding conventional fluorescence ratio images of Fluo-4/Fura Red are shown in panels B and E. These data were collected using the following settings: exposure time, 500 ms; multiplication gain, 171; frames to average, 6; and temperature, −93°. These images show that the center of the cell body is the brightest region of the cell. This is confirmed by the line profile analyses of panels C and F, which correspond to panels B and E, respectively. This cell was also photographed using a high speed imaging system comprised of a flash lamp and a synchronized ICCD camera illustrated in Figure 1. Panels G-I show single flash lamp exposures of the same cell at three time points after thresholding and ratioing the images. Panel H clearly shows enhanced Fluo-4/Fura Red ratios in the region of the uropod in this 6 $\mu$s. exposure. Panels J-L show images of compressed z-stacks made up of 100 sequential frames collected at times neighboring those of the single exposure frames in panels G-I. Again, the uropod expresses a high Fluo-4/Fura Red ratio compared to the cell body (panel K), although some enhanced signaling is noted in the forming uropod (panel J) and dissolving uropod (panel L). In panel K, some enhanced labeling is also noted near the lamellipodium. Images were processed as described above. The range of the color mask employed is shown at the right of each image. Line profile analyses were performed on the images of panels J—L as shown in panels M—O, which confirms the enhanced ratio at the uropod. (Experiments with similar findings were reproduced on 13 different days.) (bar = 5 $\mu$m).

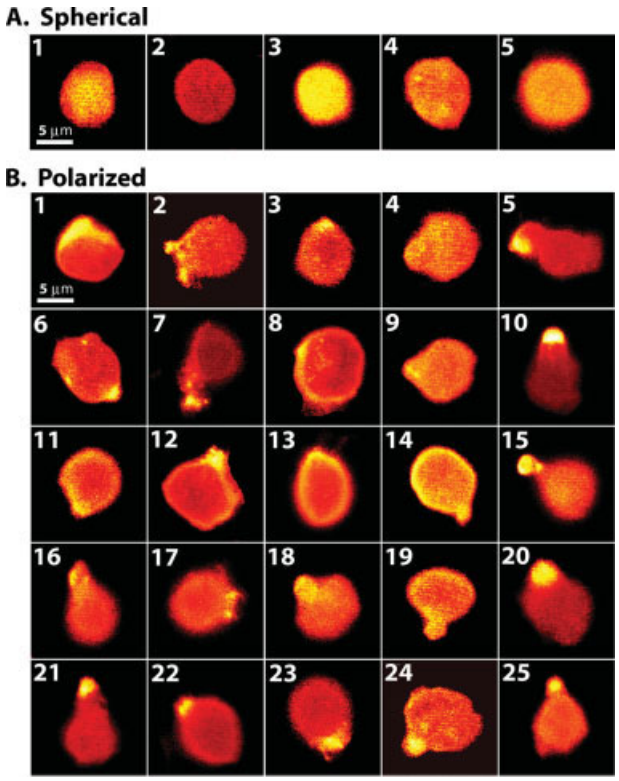


**Figure 3.** Gallery of Fluo-4/Fura Red $Ca^{2+}$ ratio micrographs using high speed illumination. Data were collected as described in Figure 1 using flash lamp illumination and simultaneous imaging of both emission wavelengths. Panel A, frames 1—5, show spherical cells. No signaling microdomains are associated with these cells. In panel B, frames 1-25, a wide range of polarized neutrophils was examined. Although cell morphologies vary somewhat, the enhanced ratio of the uropod was generally observed in well-polarized neutrophils. Poorly polarized cells displayed little uropod-specific signal (panel B, frame 4) whereas well-polarized cells (frame 10) display well-developed signaling microdomains. (The measured ratios vary from 1.1 to 2.1.) (bar = 5 $\mu$m).

based excitation tools clearly improve the contrast of $Ca^{2+}$ signaling patterns in neutrophils.

The data presented above form an in-depth analysis of calcium signaling patterns in one cell using two different methodologies. Although these data provide compelling evidence that such $Ca^{2+}$ signals exist and are dynamic in living cells, they do not illustrate the heterogeneity of cell responses. Calcium signaling patterns were not observed in spherical neutrophils under the given experimental conditions (e.g., Fig. 3A). As illustrated in Figure 2J, $Ca^{2+}$ patterns were not readily apparent in cells early as they were becoming morphologically polarized or as cells were de-polarizing. In general, cells that had a more pronounced constriction between the cell body and uropod (a well resolved ring or "neck") displayed the greatest contrast in $Ca^{2+}$ ratio. To illustrate these points, Figure 3 shows a gallery of micrographs of $Ca^{2+}$ signaling patterns in polarized human neutrophils. In all instances, the highly polarized cells displaying well-developed uropods are associated with enhanced $Ca^{2+}$ signaling.

## Discussion

In the present study we have outlined several approaches to improve the signal-to-noise ratio in ratiometric calcium imaging experiments in combination with a flash lamp excitation source to remove diffusional blurring during the exposure period. The combination of the three approaches: cutting-edge instrumentation, optimal labels and labeling strategies, and buffers optimized for physiological relevance and $Ca^{2+}$ signaling have allowed fluorescence images of $Ca^{2+}$ probes with acceptable contrast to be formed with a single 6-$\mu$s flash. Z-stacks of sequential images can be used to observe dynamic changes in signal location or, in the case of relatively stationary signal sources, can be compressed to yield high-resolution images without probe and signal diffusion or flow during the exposure period.

Previous studies by Brundage et al. (21) have shown that the uropod of polarized eosinophils displays enhanced $Ca^{2+}$ signaling. In this case, newt eosinophils, which are roughly 100 $\mu$m in size, were used. In general, studies of human neutrophils have not demonstrated $Ca^{2+}$ signaling in association with the uropod (22,23), although $Ca^{2+}$ microdomains have been noted in the case of phagocytosis (24). As newt eosinophils are over 10 times larger than human neutrophils, much longer exposure times can be used without randomizing a signal in comparison to the size of the cell. Using our imaging instrumentation and protocol, we find that the uropod of human neutrophils demonstrates high levels of $Ca^{2+}$ signaling and that the cell body demonstrates uniform calcium. Because of the brief excitation pulse delivered by the flash lamp, displacement of the probes and $Ca^{2+}$ ions during the exposure are much less than the Rayleigh criterion for microscopic resolution. Consequently, these molecules cannot move from the uropod to the cell body during the flash, which enhances the ability to localize signals. Furthermore, as the time required to download each frame is long compared to the diffusional mixing of the probe, localized $Ca^{2+}$ patterns from previous frames are randomized (or pumped down) before the next frame is acquired. Although the cell body demonstrated a high Fluo-4/Fura Red ratio using conventional imaging protocols, this is likely an artifact of the long exposure times, not an indication that $Ca^{2+}$ stores near the cell's center are discharged during cell locomotion. Indeed, plasma membrane $Ca^{2+}$ channels and $Ca^{2+}$ stores near the plasma membrane are likely participants in cell signaling. Broadly, we believe that our work is more consistent with the scientific literature than studies relying upon conventional imaging tools. Indeed, we suggest that the uropod is the location of the $Ca^{2+}$ signaling and that the slow global increase in the ratio (Fig. 2B vs. 2E and 2A vs. 2L) is not a meaningful signal. Furthermore, in our opinion, the new methodology reported above indicates that a previous nonratiometic study from this group on $Ca^{2+}$ signals is incorrect (25). Specifically, we conclude that the work of Fay and coworkers (21) is generally true for leukocytes, including human neutrophils. Moreover, it is possible that uropodial $Ca^{2+}$ signaling is a general feature of cell migration.

The accumulation of $Ca^{2+}$ at the uropod could be due to enhanced $Ca^{2+}$ delivery to the cytosol or to diminished $Ca^{2+}$ removal from the cytosol at this location. Diminished removal from the cytosol does not appear to be a likely explanation as the uropod contains a portion of the endoplasmic reticulum (26), a major site of $Ca^{2+}$ sequestration via its $Ca^{2+}$ ATPase activity. Furthermore, the cell body contains the nucleus and is rich in granules (27), suggesting that $Ca^{2+}$ removal might be somewhat slower near the center of the cell body, which could contribute to the higher ratio of the cell body using conventional ratio imaging methods.

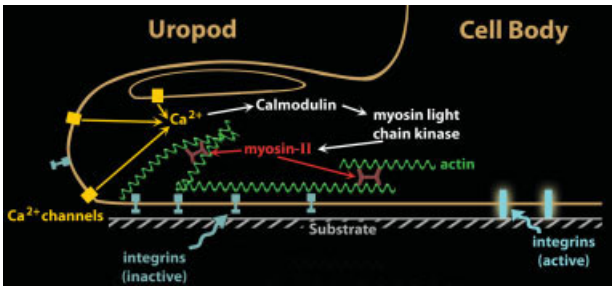


**Figure 4.** Potential model of $Ca^{2+}$ signaling at the uropod. The $Ca^{2+}$ microdomains noted above may participate in regulatory signaling, as noted in this figure.

It seems likely that the observed enhancement of $Ca^{2+}$ signaling is physiologically relevant. In the Results section we report that the measured Fluo-4/Fura Red ratio increases from 0.3 near the center of the cell body to >1.0 in the uropod. Previous studies have noted that this dye combination is difficult to calibrate due to nonlinear behavior below 500 nM (28). Therefore, it seems likely that the $Ca^{2+}$ microdomains display a concentration greater than this value. As $Ca^{2+}$ concentrations in the $\mu$M range have been associated with neutrophil functions (29), the $Ca^{2+}$ signaling patterns noted above may be involved in physiological processes.

Cell polarity is central to cell function (30). The uropod's $Ca^{2+}$ signaling function is likely linked to its role in cytoskeletal rearrangement. Previous workers have suggested that L-type $Ca^{2+}$ channels are important in controlling the contraction of the trailing tail of fibroblasts (31). More importantly, Eddy et al. (32) have shown that $Ca^{2+}$-dependent activation of myosin II is a key participant in uropod retraction by human neutrophils. These authors have used an antibody specific for the activated form of myosin II to show that this molecule is found at the uropod and leading edge of neutrophils. Activated myosin II likely participates in the retraction of the uropod and formation of the lamellipodium. Our studies indicate that $Ca^{2+}$ is preferentially located at the uropod of human neutrophils, thus likely contributing to the activation of myosin II, as schematically illustrated in Figure 4. Therefore, our findings support those of Brundage et al. (21) and Eddy et al. (32) and suggest $Ca^{2+}$ signaling patterns participate in the regulation of cell locomotion.

Although the studies reported above focus upon cell polarization, this approach should be applicable in many other situations. This is particularly true for cases in which calcium's diffusion coefficient is significant, the cells are ~10 $\mu$m, and the signals are anisotropic. For example, cell attachment to

extracellular materials and other cells may be particularly interesting. Cellular responses to ligand-coated beads is another potential area of interest. We are presently using this approach to study signaling events associated with the induction of tumor cell apoptosis.

## Literature Cited


1. Trapani JA, Sutton VR, Smyth MJ. CTL granules: Evolution of vesicles essential for combating virus infections. Immunol Today 1999;20:351–356.
2. Musiani P, Allione A, Modica A, Lollini PL, Giovarelli M, Cavallo F, Belardelli F, Forni G, Modesti A. Role of neutrophils and lymphocytes in inhibition of a mouse mammary adenocarcinoma engineered to release IL-2. IL-4, IL-7, IL-10, IFN-alpha, IFN-gamma, and TNF-alpha. Lab Invest 1996;74:146–157.
3. Davis MM, Krogsgaard M, Huppa JB, Sumen C, Purbhoo MA, Irvine DJ, Wu LC, Ehrlich L. Dynamics of cell surface molecules during T cell recognition. Annu Rev Biochem 2003;72:717–742.
4. Bromley SK, Burack WR, Johnson KG, Somersalo K, Sims TN, Sumen C, Davis MM, Shaw AS, Allen PM, Dustin ML. The immonological synapse. Annu Rev Immunol 2001;19:375–396.
5. Cartron G, Dacheux L, Salles G, Solal-Celigny P, Bardos P, Colombat P, Watier H. Therapeutic activity of humanized anti-CD20 monoclonal antibody and polymorphism in IgG Fc receptor FcγRIIIa gene. Blood 2002;99:754–758.
6. Sondel PM, Hank JA. Antibody-directed, effector cell-mediated tumor destruction. Hematol Oncol Clin North Am 2001;15:703–721.
7. Nasi E, Tillotson D. The rate of diffusion of Ca2+ and Ba2+ in a nerve cell body. Biophys J 1985;47:735–738.
8. Allbritton NL, Meyer T, Stryer L. Range of messenger action of calcium ion and inositol 1,4,5-trisphosphate. Science 1992;258:1812–1815.
9. Simon SM, Llinás RR. Compartmentalization of the submembrane calcium activity during calcium influx and its significance in transmitter release. Biophys J 1985; 48:485–498.
10. Cheek TR, O'sullivan AJ, Moreton RB, Berridge MJ, Burgoyne RD. Spatial localization of the stimulus-induced rise in cytosolic $Ca^{2+}$ in bovine adrenal chromaffin cells. Distinct nicotinic and muscarinic patterns. FEBS Lett 1989;247:429–434.
11. Monck JR, Robinson IM, Escobar AL, Vergara JL, Fernandez JM. Pulsed laser imaging of rapid $Ca^{2+}$ gradients in excitable cells. Biophys J 1994;67:505–514.
12. Robinson IM, Finnegan JM, Monck JR, Wightman RM, Fernandez JM. Colocalization of calcium entry and exocytotic release sites in adrenal chromaffin cells. Proc Natl Acad Sci USA 1995;92:2474–2478.
13. Isenberg G, Etter EF, Wendt-Gallitelli MF, Schiefer A, Carrington WA, Tuft RA, Fay FS. Intrasarcomere [Ca2+] gradients in ventricular myocytes revealed by high speed digital imaging microscopy. Proc Natl Acad Sci USA 1996;93:5413–5418.
14. O'sullivan AJ, Cheek TR, Moreton RB, Berridge MJ, Burgoyne RD. Localization and heterogeneity of agonist-induced changes in cytosolic calcium concentration in single bovine adrenal chromaffin cells from video imaging of fura-2. EMBO J 1989;8:401–411.
15. Huber-Lang M, Sarma VJ, Lu KT, McGuire SR, Padgaonkar VA, Guo RF, Younkin EM, Kunkel RG, Ding J, Erickson R, Curnutte JT, Ward PA. Role of C5a in multiorgan failure during sepsis. J Immunol 2001;166:1193–1199.
16. Bickel M, Cimasoni G. The pH of human crevicular fluid measured by a new microanalytical technique. J Periodontal Res 1985;20:35–40.
17. Gore DC, Jahoor F, Hibbert JM, DeMaria EJ. Lactic acidosis during sepsis is related to increased pyruvate production, not deficits in tissue oxygen availability. Ann Surg 1996;224:97–102.
18. Bakowski D, Parekh AB. Regulation of store-operated calcium channels by the intermediary metabolite pyruvic acid. Curr Biol. 2007;17:1076–1081.
19. Bolsover SR, Silver RA, Whitaker M. Ratio imaging microscopy of intracellular calcium and pH. In: Shotton D, editor. Electronic Light Microscopy. New York: Wiley-Liss; 1993. pp 181–210.
20. Petty HR. Fluorescence microscopy: Established and emerging methods, experimental strategies, and applications in immunology. Microsc Res Tech 2007;70:687–709.
21. Brundage RA, Fogarty KE, Tuft RA, Fay FS. Chemotaxis of newt eosinophils: Calcium regulation of chemotactic response. Am J Physiol 1993;34:C1527–C1543.
22. Marks PW, Maxfield FR. Local and global changes in cytosolic free calcium in neutrophils during chemotaxis and phagocytosis. Cell Calcium 1990;11:181–190.
23. Jacob R. Imaging cytoplasmic free calcium in histamine stimulated endothelial cells and in fMet-Leu-Phe stimulated neutrophils. Cell Calcium 1990;11:241–249.
24. Murata T, Sullivan JA, Sawyer DW, Mandell GL. Influence of type and opsonization of ingested particle on intracellular free calcium distribution and superoxide production by human neutrophils. Infect Immun 1987;55:1784–1791.
25. Kindzelskii AL, Petty HR. Intracellular calcium waves accompany neutrophil polarization, formylmethionylleucylphenylalanine stimulation, and phagocytosis: A high speed microscopy study. J Immunol 2003;170:64–72.
26. Thieblemont N, Wright SD. Transport of bacterial lipopolysaccharide to the golgi apparatus. J Exp Med 1999;190:523–534.
27. Davis BH, Walter RJ, Pearson CB, Becker EL, Oliver JM. Membrane activity and topography of F-Met-Leu-Phe-Treated polymorphonuclear leukocytes. Acute and sustained responses to chemotactic peptide. Am J Pathol 1982;108:206–216.
28. Floto RA, Mahaut-Smith MP, Somasundaram B, Allen JM. IgG-induced $Ca^{2+}$ oscillations in differentiated U937 cells: A study using laser scanning confocal microscopy and co-loaded fluo-3 and fura-red fluorescent probes. Cell Calcium 1995;18:377–389.
29. Smolen JE, Stoehr SJ, Boxer LA. Human neutrophils permeabilized with digitonin respond with lysosomal enzyme release when exposed to micromolar levels of free calcium. Biochim Biophys Acta 1986;886:1–17.
30. Sánchez-Madrid F, del Pozo MA. Leukocyte polarization in cell migration and immune interactions. EMBO J 1999;18:501–511.
31. Yang S, Huang XY. $Ca^{2+}$ influx through L-type $Ca^{2+}$ channels controls the trailing tail contraction in growth factor-induced fibroblast cell migration. J Biol Chem 2005;280:27130–27137.
32. Eddy RJ, Pierini LM, Matsumura F, Maxfield FR. $Ca^{2+}$-dependent myosin II activation is required for uropod retraction during neutrophil migration. J Cell Sci 2000;113:1287–1298.